



# A Facile Thermal-Treatment Route to Synthesize ZnO Nanosheets and Effect of Calcination Temperature

Naif Mohammed Al-Hada<sup>1\*</sup>, Elias B. Saion<sup>1</sup>, Abdul Halim Shaari<sup>1</sup>, Mazliana A. Kamarudin<sup>1</sup>, Moayad Husein Flaifel<sup>2</sup>, Sahrim Hj Ahmad<sup>2</sup>, Salahudeen A. Gene<sup>1</sup>

<sup>1</sup> Department of Physics, Faculty of Science, University Putra Malaysia, Serdang, Selangor, Malaysia, <sup>2</sup> School of Applied Physics, Faculty of Science and Technology, Universiti Kebangsaan Malaysia, Bangi, Selangor, Malaysia

## Abstract

A facile thermal-treatment route was successfully used to synthesize ZnO nanosheets. Morphological, structural, and optical properties of obtained nanoparticles at different calcination temperatures were studied using various techniques. The FTIR, XRD, EDX, SEM and TEM images confirmed the formation of ZnO nanosheets through calcination in the temperature between 500 to 650°C. The SEM images showed a morphological structure of ZnO nanosheets, which inclined to crumble at higher calcination temperatures. The XRD and FTIR spectra revealed that the samples were amorphous at 30°C but transformed into a crystalline structure during calcination process. The average particle size and degree of crystallinity increased with increasing calcination temperature. The estimated average particle sizes from TEM images were about 23 and 38 nm for the lowest and highest calcination temperature i.e. 500 and 650°C, respectively. The optical properties were determined by UV-Vis reflection spectrophotometer and showed a decrease in the band gap with increasing calcination temperature.

**Citation:** Al-Hada NM, Saion EB, Shaari AH, Kamarudin MA, Flaifel MH, et al. (2014) A Facile Thermal-Treatment Route to Synthesize ZnO Nanosheets and Effect of Calcination Temperature. PLoS ONE 9(8): e103134. doi:10.1371/journal.pone.0103134

**Editor:** Mark G. Kuzyk, Washington State University, United States of America

**Received:** April 3, 2014; **Accepted:** June 25, 2014; **Published:** August 5, 2014

**Copyright:** © 2014 Al-Hada et al. This is an open-access article distributed under the terms of the Creative Commons Attribution License, which permits unrestricted use, distribution, and reproduction in any medium, provided the original author and source are credited.

**Data Availability:** The authors confirm that all data underlying the findings are fully available without restriction. All relevant data are within the paper and its Supporting Information files.

**Funding:** The authors have no support or funding to report.

**Competing Interests:** The authors have declared that no competing interests exist.

\* Email: naifalhada@yahoo.com

## Introduction

Nanoscale particles possess several unique properties such as large surface areas, unusual adsorptive properties, surface defects and fast diffusivities. For that, this kind of nanomaterials is quite appealing in industrial and commercial applications. Recently, metal oxide nanoparticles are attractive subject of continuous scientific research and have been deeply investigated because of their physical and chemical properties as well as for their wide range of applications including sensors [1], semiconductors [2], magnetic materials [3], catalysts [4], optoelectronic materials [5], medical [6] and environmental remediation [7].

Zinc oxide (ZnO), which is a direct wideband gap semiconductor compound of the II-VI family, has a wurtzite crystalline structure at ambient conditions with hexagonal unit cell and two lattice parameters,  $a$  and  $c$ . The structure is composed of two alternating interpenetrating hexagonal closed packed (HCP) planes stacked layer-by-layer, in which each consists of oxygen anion tetrahedrally coordinated with four zinc cations at the corners of the tetrahedron along the threefold  $c$ -axis. The tetrahedral coordination of ZnO gives rise to the noncentrosymmetric structure which exhibits  $sp^3$  covalent-bonding.

Zinc Oxide (ZnO) semiconductor compound has a direct band gap of 3.37 eV at room temperature and a large excitation binding energy (60 meV), which make them promising photonic material for several applications, especially in the solid state light sources and detectors in the blue and UV spectral ranges [8]. When zinc

oxide approaches nanoscale sizes accompanied by intriguing properties due to quantum confinement effect [8] as compared to bulk counterparts, its usage can further expand to cover applications as in optical devices including blue-violet and UV-light emitting diodes [9], laser diodes [10], biosensors [11], piezoelectric transducers, solar cells [12], transparent electrodes, electroluminescent devices and photocatalytic materials [13]. Moreover, because it has been chemically and optically stable with offering low toxicity, its use as a fluorescent label for bio-imaging in medical application has been anticipated [14].

Various methods have been previously reported on the synthesis of ZnO nanosheets with improved chemical and physical properties, such as solvothermal method [15] sol-gel technique [16], precipitation method [17], hydrothermal growth (HTG) method [18], microwave assisted method [19], hydrothermal method [20], anodization method [21], thermal decomposition and reduction method [22]. Further methods also have been reported to synthesize ZnO nanoparticles such as Microemulsion method [23–26], microwave method [27], thermal evaporation [28], mechanochemical synthesis method [29], spray pyrolysis [25] and chemical vapour deposition [30]. However, most of the methods are difficult to employ in a large scale production due to the complicated procedures involved, longer reaction times, high reaction temperatures, and the involvement of toxic reagents and by-products in these synthesis methods.

In this study, thermal-treatment method was used to synthesize zinc oxide nanosheets from an aqueous solution containing only

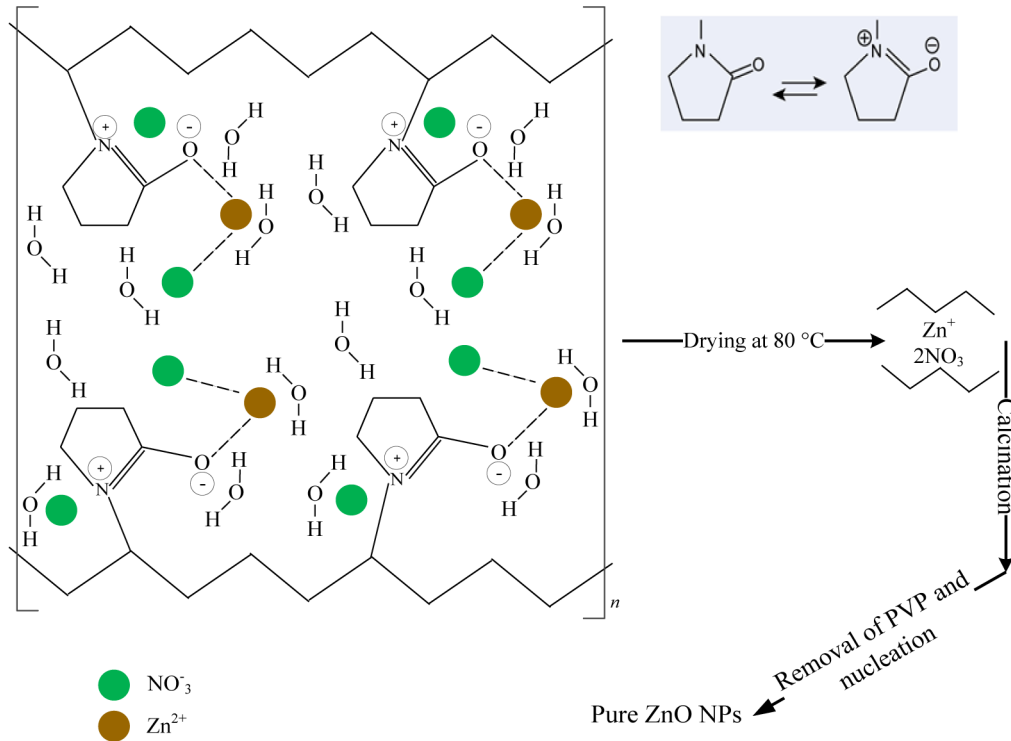


**Figure 1. A proposed mechanism of the interaction between metallic ions and PVP.**  
 doi:10.1371/journal.pone.0103134.g001

zinc nitrate, polyvinyl pyrrolidone (PVP) and deionized water. This method has the advantages of being simple, less expensive, has no unwanted by-products, and is environmentally friendly

[31,32]. The effect of calcination temperature on the structural and optical properties of ZnO nanosheets was also investigated and discussed in detail.

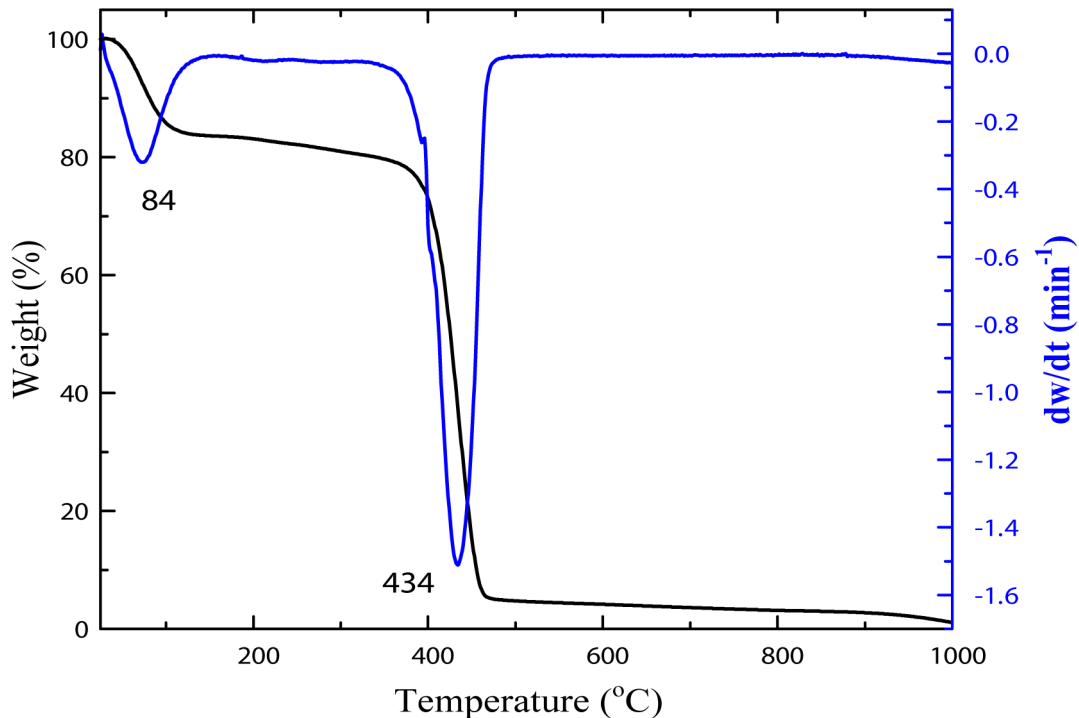


**Figure 2. Thermogravimetric (TG) and thermogravimetric derivative (DTG) curves for PVP at a heating rate of 10 °C/min.**  
 doi:10.1371/journal.pone.0103134.g002

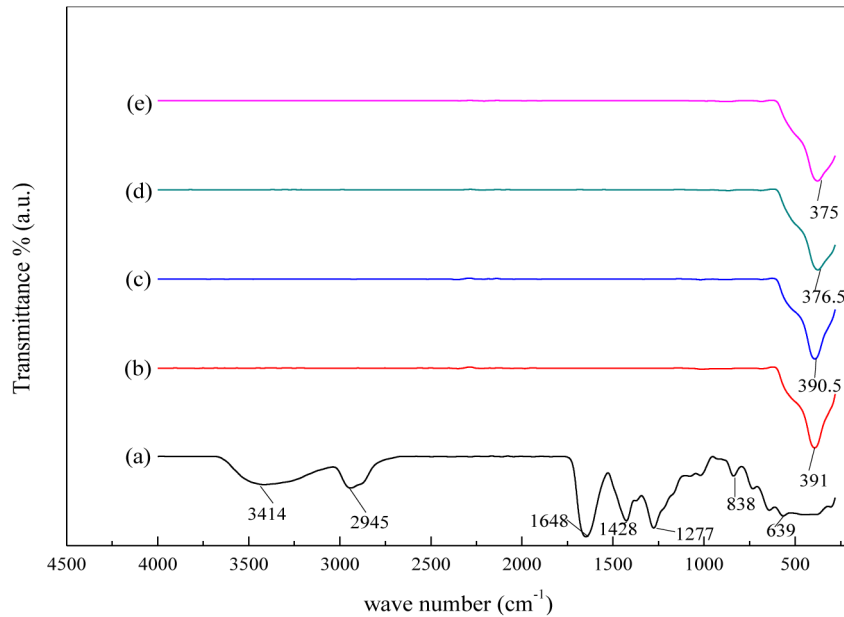


**Figure 3. FTIR spectra of (a) PVP and ZnO nanosheets at (a) 30, (b) 500, (c) 550, (d) 600, and (e) 650°C in the range of 280–4500  $\text{cm}^{-1}$ .**

doi:10.1371/journal.pone.0103134.g003

## Experimental Section

### 1. Materials

Poly (vinyl pyrrolidone) (PVP  $M_w = 29000$  g/mol) was purchased from Sigma Aldrich and utilized as a capping agent which is anticipated to stabilize the nanoparticles and hence reduce their agglomeration. Zinc nitrate reagent,  $\text{Zn}(\text{NO}_3)_2 \cdot 6\text{H}_2\text{O}$  ( $M_w = 297.47$  g/mol) and deionized water were supplied by Acros Organics SIGMA and used as metal precursor and solvent, respectively. The chemical materials were above 99% in purity and used without further purification.

### 2. Synthesis of nanosheets

The PVP solution was made by dissolving 3 g of PVP powder in 100 ml of deionized water at a temperature of 70°C in a water-bath and allowed to stir for 2 hrs. Later, zinc nitrate of 0.2 mmol was added into 100 ml PVP solution and the mixture was stirred continuously for 2 hrs until a colourless solution was obtained. No precipitation of materials was observed in the solution before it was poured in Petri dish and dried at 80°C for 24 hrs. The resulting solid was crushed for 30 min in a mortar to form powder. The powder was subsequently divided into five portions and each portion was placed in a crucible alumina to be calcined at a

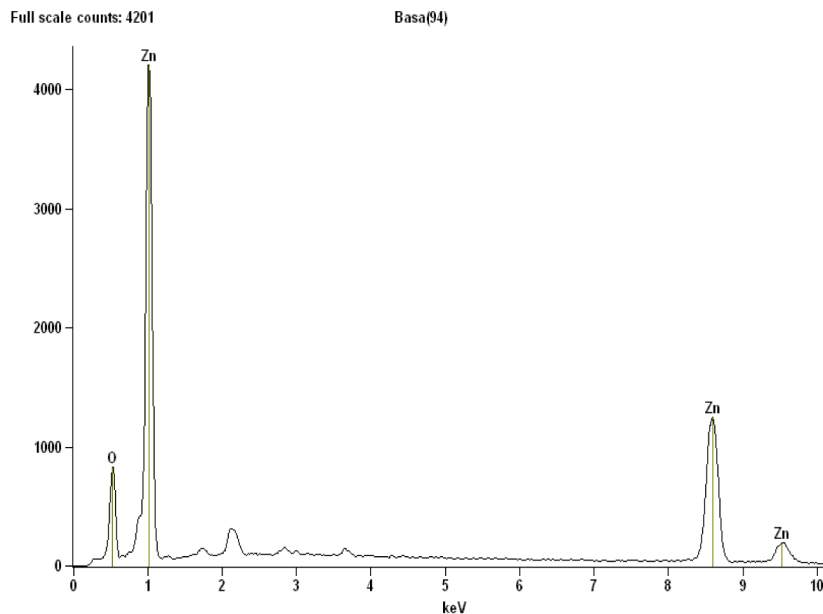


**Figure 4. The EDX spectrum of the ZnO nanosheets calcined at 500°C.**

doi:10.1371/journal.pone.0103134.g004

specific temperature for 3 hrs in order to crystalize the nanosheets and decompose the organic compounds.

### 3. Characterization

Several techniques were employed to investigate the synthesised ZnO nanosheets. The structure of ZnO nanosheets has been examined by X-ray diffractometry (XRD Shimadzu model 6000) using Cu K $\alpha$  (0.154 nm) as a radiation source to generate diffraction patterns from the crystalline powder samples at ambient temperature in  $2\theta$  range of  $10^\circ$ – $90^\circ$ . Infrared spectra ( $280$ – $4000$   $\text{cm}^{-1}$ ) have been recorded using Fourier transform infrared spectrometer (FTIR Perkin Elmer model 1650) to confirm the removal of capping agent after calcination. Basically, both XRD and FTIR results were used to prove the formation of crystalline ZnO powder at different calcination temperatures. The morphology, particle size, particle size distribution and the homogeneity of the nanosheets were determined using transmission electron microscopy (JEOL TEM model 2010F UHR) with an accelerating voltage of 200 kV. Moreover, UV–vis spectrophotometer (Shimadzu model UV-3600) was used in order to evaluate the optical properties of the samples at room temperature in the range of 200–800 nm.

## Results and Discussion

### 1. Formation mechanism of ZnO nanosheets

**Figure 1** shows a proposed interaction mechanism between Zn metallic ions and PVP. The zinc nitrate  $\text{Zn}(\text{NO}_3)_2 \cdot 6\text{H}_2\text{O}$  was added to the aqueous solution of PVP and deionized water (DI) in which it was completely dissolved. In fact, while mixing the solution, the metallic ions subdued an entrapment with amine group in the polymeric chains through ionic-dipole interactions. This was followed by a mobility congealment of the metallic cations in the polymer cavity as a result of water removal when the mixture was dried. After calcination being applied, the PVP content and undesired anions were completely removed from the

sample and gradually high purity ZnO nanosheets begun to conform with increasing calcination temperature. It is believed that PVP agent has played a role in the nucleation of ZnO nanosheets and has been a controller for the particle's size growth [33].

### 2. TGA-DTG measurements

Thermogravimetric analysis and its derivative form (TGA-DTG curves) were used so as to determine the appropriate starting temperature for the calcination process. **Figure 2** shows the thermogram of percentage weight change as a function of temperature for the sample before calcination. It is evident that the sample exhibited two step degradation processes. The first step shows insignificant weight loss occurred at an initial degradation temperature of  $84^\circ\text{C}$ , which is attributed to the trapped moisture in the sample. The second one demonstrates a maximum weight loss occurred at a temperature of  $434^\circ\text{C}$ , which corresponds to almost complete decomposition of PVP in the sample. At  $485^\circ\text{C}$ , the weight loss change as a function of temperature became insignificant as most of the PVP content in the sample turned to carbonaceous products and hence leaving pure metal oxide nanosheets of the sample as the final residue [33].

### 3. Phase and elemental composition analysis

FTIR spectroscopy helps analysing multi-component systems and provides necessary information pertaining the material's phase composition and types of interactions existing amongst various kinds of polymers. In our study, FTIR measurement was employed to determine the appropriate calcination temperature at which pure crystal nanosheets conform with no organic agent trace being detected. This further can be evidenced through investigating the interaction between ZnO nanosheets and PVP at different calcination temperatures using TEM images. The FTIR spectra show the organic and inorganic contents of the sample before and after being calcined over the wave number range of  $280$ – $4000$   $\text{cm}^{-1}$ . **Figure 3 (a)** exhibits all absorption peaks that

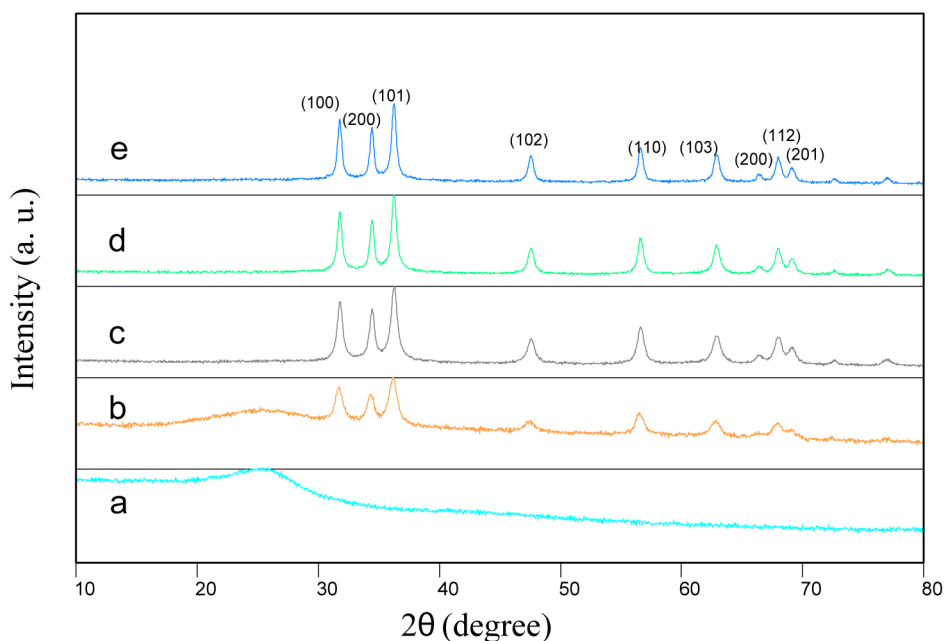


**Figure 5.** XRD patterns of zinc oxide nanosheets with different calcination temperatures of (a) room temperature, (b) 500, (c) 550, (d) 600, and (e)  $650^\circ\text{C}$ .

doi:10.1371/journal.pone.0103134.g005

**Table 1.** Briefing of the structural and optical properties of synthesized ZnO nanosheets at different calcination temperatures.

Temperature (°C)	$2\theta \pm 0.001$	$\text{FWHM} \pm 0.001$	$d$ (nm)	$D_{\text{XRD}}$ (nm)	$D_{\text{TEM}}$ (nm)	$E_g$ (eV)
500	36.22	0.36	2.4799	24	$23 \pm 2$	3.26
550	36.23	0.32	2.4796	27	$26 \pm 3$	3.25
600	36.37	0.28	2.4756	31	$30 \pm 2$	3.24
650	36.39	0.21	2.4744	41	$38 \pm 4$	3.23

doi:10.1371/journal.pone.0103134.t001

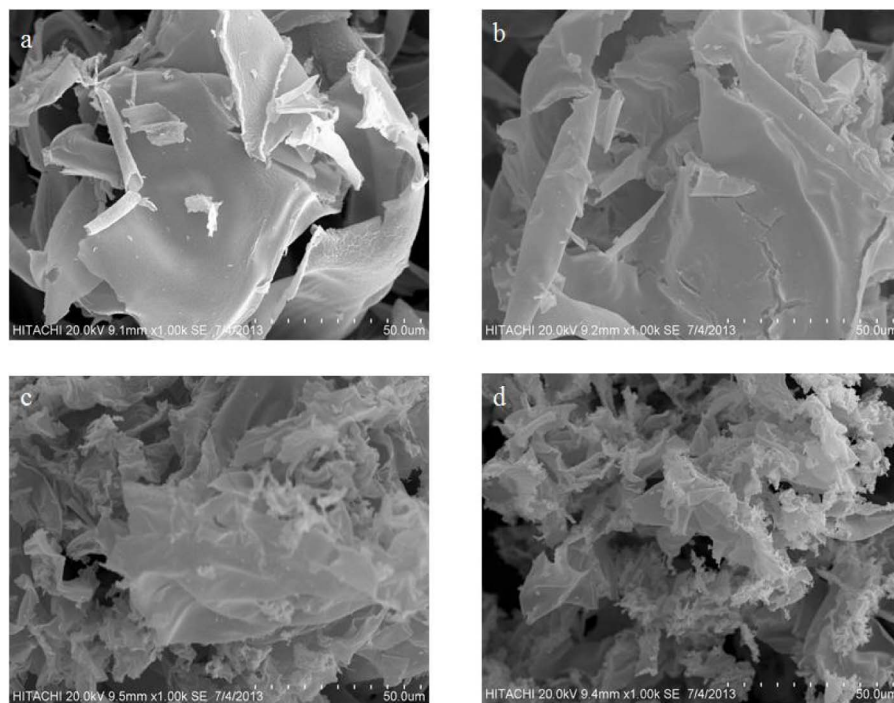
are attributed to the PVP and ZnO nanosheets. Before calcination the absorption peaks at wave number of 3414, 2945 and  $1646 \text{ cm}^{-1}$  were assigned to N–H, C–H and C=O stretching vibrations, respectively. Further, the absorption peak found at  $1428 \text{ cm}^{-1}$  was ascribed to C–H bending vibration originated from methylene group, while  $1277 \text{ cm}^{-1}$  was associated with C–N stretching vibration. Finally, 839 and  $639 \text{ cm}^{-1}$  were corresponding to the vibrations occurred due to C–C ring and C–N=O bending [34]. The calcination at  $500^\circ\text{C}$  resulted in the disappearance of broadband absorption peaks that belong to the organic composition of PVP as evident in **Figure 3 (b,c,d,e)**. The vibrational spectra of ZnO nanosheets samples were observed as absorption at the wave number of 391, 385,  $376 \text{ cm}^{-1}$  and  $375 \text{ cm}^{-1}$  calcined at 500, 550,  $600^\circ\text{C}$  and  $650^\circ\text{C}$ , respectively. The presence of single absorption peak and the observed shift in the wave number for ZnO nanosheets spectra with increasing calcination temperature imply that high purity ZnO nanosheets have been obtained using thermal-treatment method.

The elemental composition of the nanosheets sample formed by thermal-treatment technique was determined using energy dispersive X-ray (EDX) spectroscopy. EDX spectrum of ZnO nanosheets calcined at  $500^\circ\text{C}$  is illustrated in **figure 4**. From the

spectrum, the Zn and O elements are vividly present in the prepared sample as shown by their respective peaks. The recorded atomic percentages of Zn and O were approximately 50.13% and 49.87%, respectively. This result indicated that the final product is pure ZnO nanosheets.

#### 4. Structural analysis

**Figure 5** shows typical XRD patterns of the samples before and after calcination. A broad spectrum exhibited by the sample before calcination indicates that the dried samples demonstrated an amorphous behaviour although physically appeared to behave like crystalline materials. For the calcined samples at  $500^\circ\text{C}$  and above, the spectrum shows sharper and narrower diffraction peaks, implying that the crystalline ZnO nanosheets formation has been established. Further, higher values of calcination temperatures were observed to enhance the crystallinity of the ZnO nanosheets by increasing the intensity of the peaks and removing the undesired small peaks appeared at lower calcination temperatures. This crystallinity enhancement with increasing calcination temperatures is stemmed from the increment of the crystalline volume to surface ratio, as evidenced by TEM images, which occurred due to particle size enlargement. From **Table 1**, it is also

**Figure 6.** SEM images of ZnO nanosheets at calcination temperatures of (a) 500 and (b) 550, (c) 600 and (d)  $650^\circ\text{C}$ .

doi:10.1371/journal.pone.0103134.g006

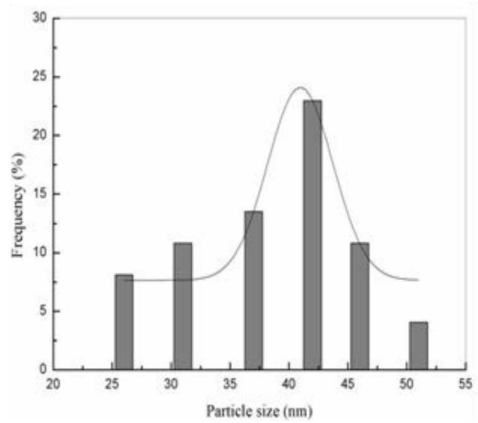
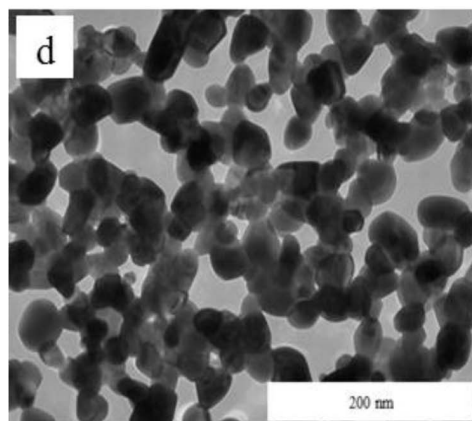
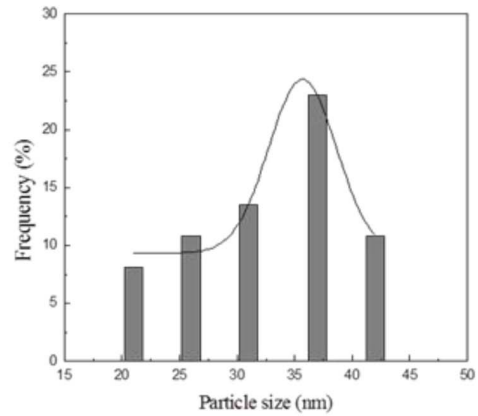
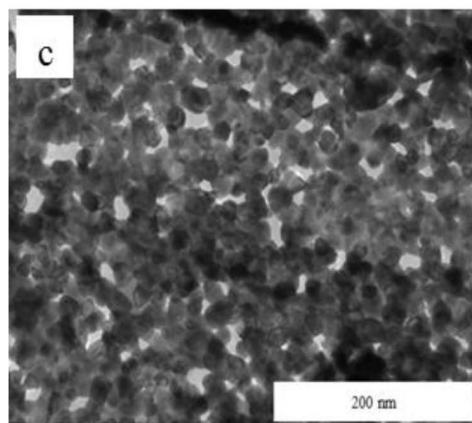
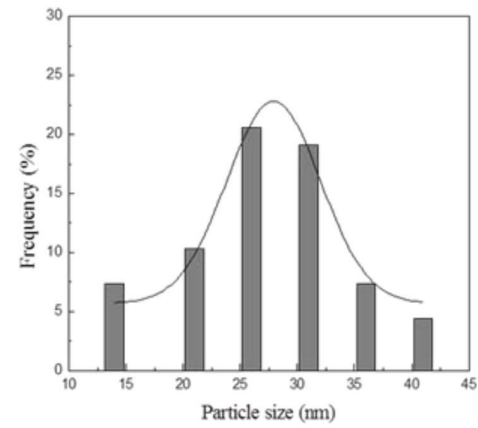
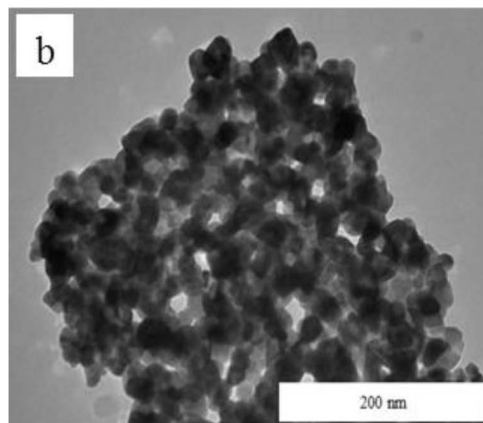
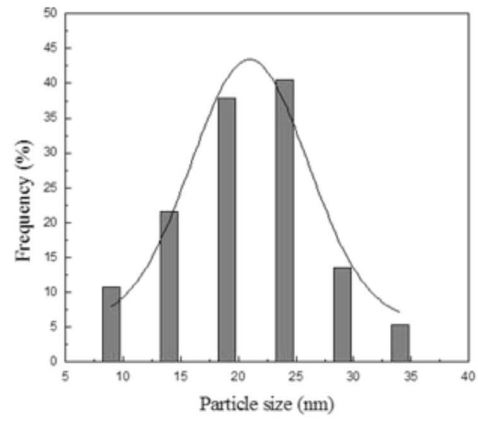
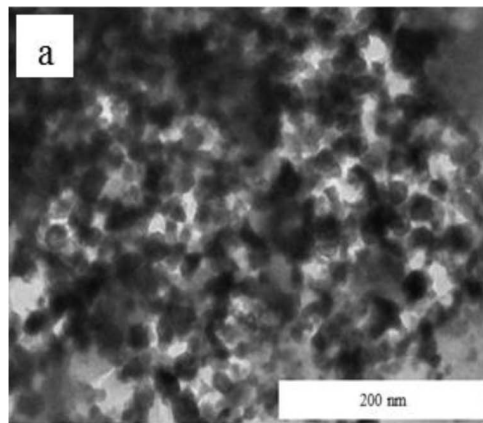


**Figure 7. TEM images and particle size distribution of ZnO nanosheets at calcination temperature of (a) 500, (b) 550, (c) 600 and (d) 650°C.**

doi:10.1371/journal.pone.0103134.g007

apparent that the d-spacing has decreased with increasing calcination temperatures. The position of the Bragg's lines of ZnO nanosheets was used to determine the interplaner spacing ( $d$ ), which in turn used to index the diffraction peaks. The existence of multiple diffraction peaks of (100), (200), (101), (102), (110), (103),(200),(112) and (201) in the diffraction patterns suggests that the ZnO samples have a typical hexagonal structure referring to JCPDS card no. 36-1451 data [32,35]. The samples' crystallite sizes were found to range from 24 to 41 nm, which were calculated for the most intense peak (101) using the Scherrer's equation as given below;

$$D = 0.9 \lambda / \beta \cos \theta \quad (1)$$

where  $D$  is the crystallite size (nm),  $\beta$  is the full width of the diffraction line at half of the maximum intensity i.e. (101) which is measured in radians,  $\lambda$  is the X-ray wavelength of Cu  $K\alpha = 0.154$  nm and  $\theta$  is the Bragg's angle [1].

## 5. Morphological examination

The surface morphology of ZnO nanosheets were demonstrated using scanning electron microscopy (SEM). **Figure 6**, shows SEM images of ZnO nanosheets and the calcination temperature's effect. The results are in agreement with previously reported literature [19,22,36]. **Figure 6(a) and (b)** reveal that the product has a nanosheet appearance with a shrunken edges and irregular morphology structure at low temperature. However, ZnO nanosheet product gradually started to crumble and overlapped in a proportional relation with the increment of calcination temperature as shown in **figure 6 (c) and (d)**.

Transmission electron microscopy (TEM) images were used to demonstrate the morphology, particle size and particles' size distribution of ZnO nanoparticles and are shown in **figure 7 (a),**

**(b), (c) and (d)**. The obtained images show that the ZnO sample prepared by thermal-treatment method has exhibited uniform morphology and good particle size distribution. The average particle size at calcination temperatures of 500, 550, 600 and 650°C is about 23, 26, 30 and 38 nm, respectively, which were found to be in good agreement with the XRD measurements. These results indicate that the attained particle size has increased with increasing calcination temperature due to the fact that as the temperature went high, many neighbouring particles were prone to fuse together to form larger particle sizes by melting their surfaces [37].

## 6. Optical properties

Diffuse reflectance spectra are normally determined by a UV-visible spectrophotometer. The diffuse reflectance technique is capable of collecting the reflected light flux after interacting with the targeted sample. Then, the technique compares the reflected light fluxes coming from the surfaces of targeted sample and the standard reference sample.

In order to investigate the calcination effect on the optical properties of ZnO nanosheets, the diffuse reflectance spectra, as shown in **figure 8**, were measured in the range of 200–800 nm at room temperature for all calcined samples. The optical band gap values for all samples calcined at different temperatures were determined from reflectance spectra using Kubelka-Munk equation;

$$(F(R_{\infty}).hv)^2 = (A.(hv - E_g)) \quad (2)$$

where  $F(R_{\infty})$  is the so-called remission parameter or Kubelka-Munk function,  $hv$  is the incident photon energy,  $A$  is a constant depending on the transition probability and the diffuse reflectance  $R_{\infty}$ ,  $R_{\infty}$  is the diffuse reflectance that is obtained from

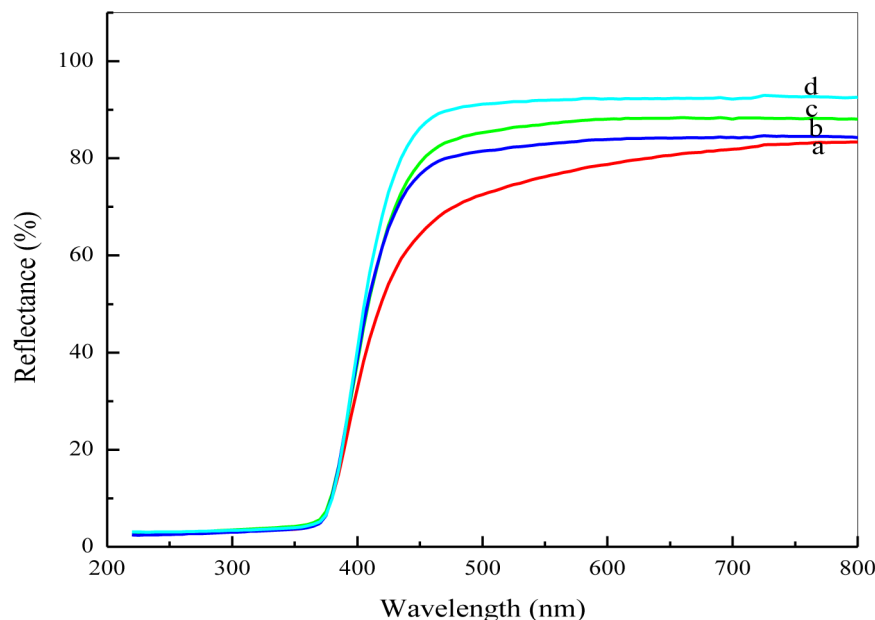


**Figure 8. Reflectance of ZnO nanosheets calcined at different temperatures of (a) 500 (b) 550 (c) 600 (d) 650°C.**

doi:10.1371/journal.pone.0103134.g008

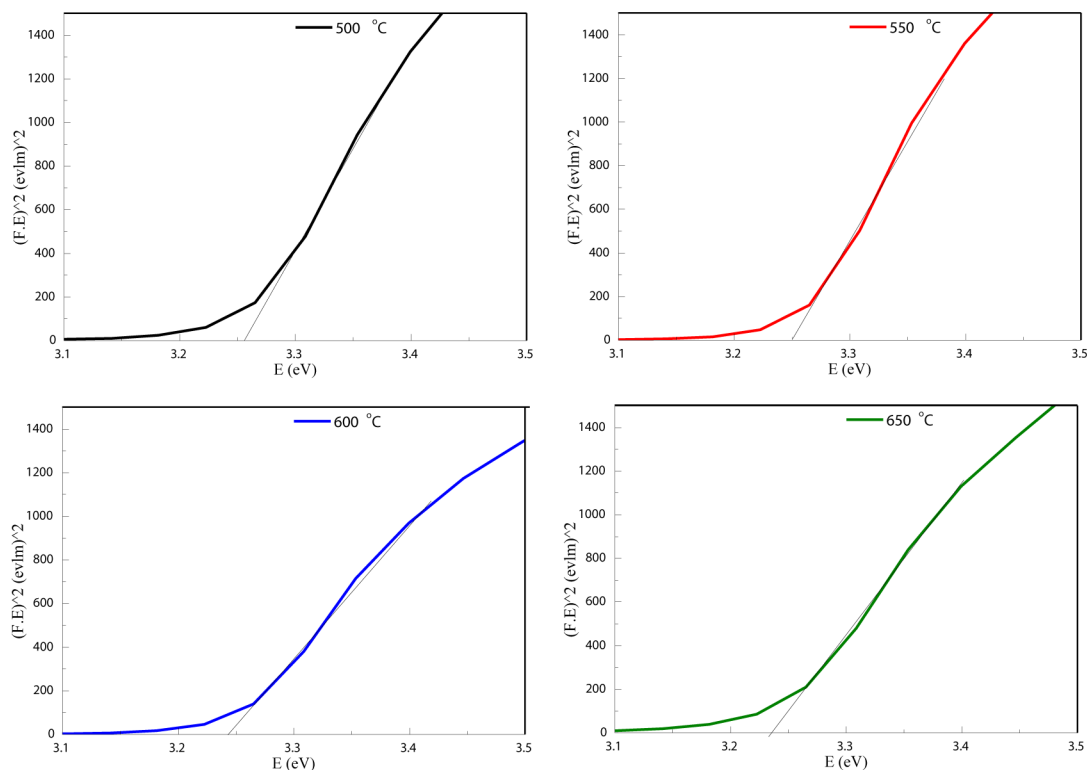


**Figure 9. The method of extracting the band gaps of ZnO nanosheets calcined at different temperatures.**  
doi:10.1371/journal.pone.0103134.g009

$R_{\infty} = R_{\text{sample}}/R_{\text{standard}}$  [38]. The values of  $(F(R_{\infty}) \cdot h\nu)^2$  versus  $(h\nu)$  were plotted as illustrated in **figure 9**. Straight lines were drawn to fit the experimental band gap curves and were extended to intercept the  $(h\nu)$  axis in order to determine the optical band gap values of the ZnO nanosheets at different calcination temperatures. It was found that the optical band gap has decreased with increasing calcination temperature from 3.260 eV at 500°C to 3.23 eV at 650°C as shown in **Table 1**. A decrease in the energy band gap with increasing calcination temperatures is attributed to the increase in the particle size as well as to crystallinity improvement, as was evidenced by XRD analysis. It is believed that as the particle size increases, the number of atoms that form a particle also increase, which consequently render the valence and conduction electrons more attractive to the ions core of the particles and hence decreasing the band gap of the particles.

## Conclusions

ZnO nanosheets have been successfully synthesized by thermal-treatment method using only zinc nitrate as metal precursor, PVP as a capping agent and deionized water as a solvent. The calcination has enabled the removal of organic compounds and nitrate ions leaving a residue of pure crystalline ZnO nanosheets.

## References

- Park CO, Akbar SA, Weppner W (2003) Ceramic electrolytes and electrochemical sensors. *J Mater Sci* 38: 4639–4660.
- Kuzmik J, Konstantinidis G, Harasek S, Haščik Š, Bertagnolli E, et al. (2004) ZnO 2/(Al)GaN metal oxide–semiconductor structures: characterization and application. *Semicond Sci Technol* 19: 1364.
- Prodan AM, Iconaru SL, Chifiriuc CM, Bleotu C, Ciobanu CS, et al. (2013) Magnetic Properties and Biological Activity Evaluation of Iron Oxide Nanoparticles. *J Nanomater* 2013: 7.
- Alghamdi K, Hargreaves JSJ, Jackson SD (2009) Base Catalysis with Metal Oxides. *Metal Oxide Catalysis: Wiley-VCH Verlag GmbH & Co. KGaA*: 819–843.
- Kalyanasundaram K, Grätzel M (1998) Applications of functionalized transition metal complexes in photonic and optoelectronic devices. *Coord Chem Rev* 177: 347–414.
- Premanathan M, Karthikeyan K, Jayasubramanian K, Manivannan G (2011) Selective toxicity of ZnO nanoparticles toward Gram-positive bacteria and

The average particle size decreased from 23 to 38nm when increasing calcination temperature from 500 to 650°C, respectively. The band gap energy of ZnO nanosheets has been determined from the reflectance spectra and found decreasing from 3.260 eV at 500°C to 3.23 eV at 650°C. The thermal-treatment method is proven to be a simple and low cost method to synthesize ZnO nanosheets with high purity and also being friendly to the environment because of lack of chemical reagents used and no toxic by-product effluents.

## Acknowledgments

The authors would like acknowledge technical supports from the staff of the Faculty of Science and the Institute of Bioscience at UPM and UKM in this work.

## Author Contributions

Conceived and designed the experiments: NMA ES AHS MAK. Performed the experiments: NMA MHF. Analyzed the data: NMA ES MHF SHA. Contributed reagents/materials/analysis tools: NMA ES MAK MHF SHA SAG. Contributed to the writing of the manuscript: NMA ES AHS MHF SAG.



- cancer cells by apoptosis through lipid peroxidation. *Nanomed Nanotechnol Biol Med* 7: 184–192.
7. Oskam G (2006) Metal oxide nanoparticles: synthesis, characterization and application. *J Sol-Gel Sci Technol* 37: 161–164.
  8. Lin K-F, Cheng H-M, Hsu H-C, Lin L-J, Hsieh W-F (2005) Band gap variation of size-controlled ZnO quantum dots synthesized by sol-gel method. *Chemical Physics Letters* 409: 208–211.
  9. Wang ZL (2008) Splendid one-dimensional nanostructures of zinc oxide: A new nanomaterial family for nanotechnology. *ACS Nano* 2: 1987–1992.
  10. Joseph DP, Venkateswaran C (2011) Bandgap Engineering in ZnO By Doping with 3d Transition Metal Ions. *J Atom Mol Phys* 2011: 7
  11. Topoglidis E, Cass AEG, O'Regan B, Durrant JR (2001) Immobilisation and bioelectrochemistry of proteins on nanoporous TiO<sub>2</sub> and ZnO films. *J Electroanal Chem* 517: 20–27.
  12. Srivastava V, Gusain D, Sharma YC (2013) Synthesis, characterization and application of zinc oxide nanoparticles (n-ZnO). *Ceram Int* 39: 9803–9808.
  13. Lin H-M, Tzeng S-J, Hsiao P-J, Tsai W-L (1998) Electrode effects on gas sensing properties of nanocrystalline zinc oxide. *Nanostruct Mater* 10: 465–477.
  14. Tachikawa S, Noguchi A, Tsuge T, Hara M, Odawara O, et al. (2011) Optical Properties of ZnO Nanoparticles Capped with Polymers. *Mater* 4: 1132–1143.
  15. Pan A, Yu R, Xie S, Zhang Z, Jin C, et al. (2005) ZnO flowers made up of thin nanosheets and their optical properties. *J Cryst Growth* 282: 165–172.
  16. Zhao X, Lou F, Li M, Lou X, Li Z, et al. (2014) Sol-gel-based hydrothermal method for the synthesis of 3D flower-like ZnO microstructures composed of nanosheets for photocatalytic applications. *Ceram Int* 40: 5507–5514.
  17. Huang XH, Guo RQ, Wu JB, Zhang P (2014) Mesoporous ZnO nanosheets for lithium ion batteries. *Mater Lett* 122: 82–85.
  18. Tsai F-S, Wang S-J (2014) Enhanced sensing performance of relative humidity sensors using laterally grown ZnO nanosheets. *Sensor Actuat B-Chem* 193: 280–287.
  19. Sahoo S, Barik SK, Gaur A, Correa M, Singh G, et al. (2012) Microwave Assisted Synthesis of ZnO Nano-Sheets and Their Application in UV-Detector. *ECS J Solid State Sci Technol* 1: Q140–Q143.
  20. Elkhidir Suliman A, Tang Y, Xu L (2007) Preparation of ZnO nanoparticles and nanosheets and their application to dye-sensitized solar cells. *Sol Energy Mater Sol Cells* 91: 1658–1662.
  21. Zhao J, Wang X, Liu J, Meng Y, Xu X, et al. (2011) Controllable growth of zinc oxide nanosheets and sunflower structures by anodization method. *Mater Chem Phys* 126: 555–559.
  22. Hu JQ, Bando Y, Zhan JH, Li YB, Sekiguchi T (2003) Two-dimensional micrometer-sized single-crystalline ZnO thin nanosheets. *Appl Phys Lett* 83: 4414–4416.
  23. Singhal M, Chhabra V, Kang P, Shah D (1997) Synthesis of ZnO nanoparticles for varistor application using Zn-substituted aerosol OT microemulsion. *Mater Res Bull* 32: 239–247.
  24. Sarkar D, Tikku S, Thapar V, Srinivasa RS, Khilar KC (2011) Formation of zinc oxide nanoparticles of different shapes in water-in-oil microemulsion. *Colloids Surf., Physicochem Eng Asp* 381: 123–129.
  25. Zhao X, Zheng B, Li C, Gu H (1998) Acetate-derived ZnO ultrafine particles synthesized by spray pyrolysis. *Powder Technol* 100: 20–23.
  26. Li X, He G, Xiao G, Liu H, Wang M (2009) Synthesis and morphology control of ZnO nanostructures in microemulsions. *J Colloid Interface Sci* 333: 465–473.
  27. Komarneni S, Bruno M, Mariani E (2000) Synthesis of ZnO with and without microwaves. *Mater Res Bull* 35: 1843–1847.
  28. Dai ZR, Pan ZW, Wang ZL (2003) Novel nanostructures of functional oxides synthesized by thermal evaporation. *Adv Funct Mater* 13: 9–24.
  29. Tsuzuki T, McCormick PG (2001) ZnO nanoparticles synthesised by mechanochemical processing. *Scripta Mater* 44: 1731–1734.
  30. Park WI, Lee CH, Chae JH, Lee DH, Yi GC (2009) Ultrafine ZnO nanowire electronic device arrays fabricated by selective metal-organic chemical vapor deposition. *Small* 5: 181–184.
  31. Goodarz Naseri M, Saion EB, Kamali A (2012) An Overview on Nanocrystalline ZnFe 2 O 4, MnFe 2 O 4, and CoFe 2 O 4 Synthesized by a Thermal Treatment Method. *ISRN Nanotechnol* 2012: 11.
  32. Al-Hada NM, Saion E, Shaari A, Kamarudin M, Gene SA (2014) The Influence of Calcination Temperature on the Formation of Zinc Oxide Nanoparticles by Thermal-Treatment. *Appl Mech Mater* 446: 181–184.
  33. Naseri MG, Saion EB, Ahangar HA, Shaari AH (2013) Fabrication, characterization, and magnetic properties of copper ferrite nanoparticles prepared by a simple, thermal-treatment method. *Mater Res Bull* 48: 1439–1446.
  34. Giri N, Natarajan R, Gunasekaran S, Shreemathi S (2011) 13 C NMR and FTIR spectroscopic study of blend behavior of PVP and nano silver particles. *Arch Appl Sci Res* 3: 624–630.
  35. Cunha DM, Souza FL (2013) Facile synthetic route for producing one-dimensional zinc oxide nanoflowers and characterization of their optical properties. *J Alloys Compd* 577: 158–164.
  36. Zhang S-L, Lim J-O, Huh J-S, Noh J-S, Lee W (2013) Two-step fabrication of ZnO nanosheets for high-performance VOCs gas sensor. *Current Appl Phys* 13, Supplement 2: S156–S161.
  37. Maaz K, Karim S, Mumtaz A, Hasanain SK, Liu J, et al. (2009) Synthesis and magnetic characterization of nickel ferrite nanoparticles prepared by co-precipitation route. *J Magn Magn Mater* 321: 1838–1842.
  38. Torrent J, Barr'on V (2002) *Encyclopedia of Surface and Colloid Science*. Inc.:New York: Marcel Dekker 2002: 1438–1446.